JOURNAL OF SPACECRAFT AND ROCKETS
Vol. 37, No. 5, September–October 2000

Analytical Off-Design Lift-to-Drag-Ratio Analysis for Hypersonic Waveriders

Ryan P. Starkey* and Mark J. Lewis†
University of Maryland, College Park, Maryland 20742

An analytical, power-law-derived, waverider wing theory model is developed for studying the lift-to-drag-ratio characteristics of a rocket-powered waverider with a two-dimensional (planar) shock structure. Some inherent benefits of the modeling method are explored, such as the decoupling of the vehicle length and planform shape from the other components in the lift-to-drag-ratio equation. Other factors affecting lift-to-drag ratio are also investigated, including off-design angle-of-attack performance and sensitivity, off-design Mach number performance, altitude effects, base-pressure considerations, length-scale effects, and planform bluntness effects (i.e., spatulate- vs caret-style waverider configurations). The vehicle aerodynamics are derived in a manner that results in a similarity solution in which all results are independent of the width of the vehicle. This similarity allows for easy vehicle scaling once a desirable configuration has been determined.

Nomenclature

A, B	=	power-law scaling parameters
D	=	drag, N
F	=	planform scaling function
G	=	flight condition function
h	=	height, m
L	=	lift, N
l	=	length, m
M	=	Mach number
n	=	power-law exponent
P	=	pressure, Pa
S	=	area, m^2
U	=	velocity, m/s
V	=	volume, m^3
w	=	width, m
X, Y	=	lift-to-drag-ratio functions
x, y, z	=	linear dimensions, m
Z	=	altitude, km
α	=	angle of attack, deg
β	=	oblique shock inclination angle, deg
θ	=	vehicle wedge angle, deg
μ	=	kinematic viscosity, N s/m^2
ρ	=	density, kg/m^3
Ψ	=	lift-to-drag-ratio functions

Subscripts

b	=	value for base surface
c	=	value for compression surface
e	=	property at edge of boundary layer
l	=	value for lower surface
lam	=	laminar
p	=	planform
surf	=	surface inclination angle
turb	=	turbulent
u	=	value for upper surface
v	=	viscous
w	=	wall value or wetted surface area
∞	=	freestream value or surface

Superscript

$*$	=	evaluated at the reference temperature

Received 30 September 1999; revision received 10 March 2000; accepted for publication 16 March 2000.

*Graduate Research Assistant, Department of Aerospace Engineering; rstarkey@eng.umd.edu. Student Member AIAA.

†Professor, Department of Aerospace Engineering; lewis@eng.umd.edu. Associate Fellow AIAA.

Introduction

ALTHOUGH there are many factors affecting the design and optimization of hypersonic waveriders, one of the most fundamental figures of merit is the lift-to-drag (L/D) ratio. Maximizing a vehicle L/D ratio is important because it generally is equated to increased range that is often a key driving parameter behind any vehicle design. This paper investigates the effects of many design criteria on the L/D ratio and offers insight on how to maximize their effectiveness for a given mission. Some of the more basic design questions looked into are 1) how long the vehicle should be, 2) what planform shape the vehicle should have, 3) what vehicle wedge angles provide relative insensitivity to flight-path perturbations, 4) how sensitive the vehicle design is to variations in base pressure (i.e., engine on or off), and 5) the effects of off-design Mach number and angle of attack.

Use of a simple parametric vehicle model allows for studies of many different design variables and fundamental optimization tradeoffs with modest computational effort. Furthermore, the power-law-shaped waverider with a two-dimensional shock structure used for this study defines all aerodynamic and geometric parameters analytically for increased simplicity. Using this simple model, we explore the tradeoffs involved with optimizing a Mach 8 waverider for the maximum L/D ratio at a cruising altitude of 20 km.

Vehicle Model

A waverider with a two-dimensional (planar) shock is generated by use of power-law equations to define the curvatures of both the planform p and upper u surfaces:

$$y_p = Ax^n \tag{1}$$

$$y_u = B(z_u)^n \rightarrow z_u = (y_u/B)^{1/n} \tag{2}$$

where the zero coordinate point is at the nose centerline with the height defined as positive going down, as shown in Fig. 1. Parameters A and B are positive scaling constants, and the exponent n can vary within the range 0–1.

To ensure vehicles with a wedge-derived flowfield, i.e., a planar shock, the vehicle must have a constant wedge angle θ at every spanwise location. When the curvature of the lower surface is constrained to follow the equation

$$\tan\theta = \frac{z_l - (y_u/B)^{1/n}}{x - (y_p/A)^{1/n}} \tag{3}$$

a planar shock is guaranteed.

The vehicle upper surface is generated by the application of Eq. (1) between $x = 0$ and the desired vehicle length $x = l$ along with Eq. (2). Similarly, the vehicle lower surface is generated by the

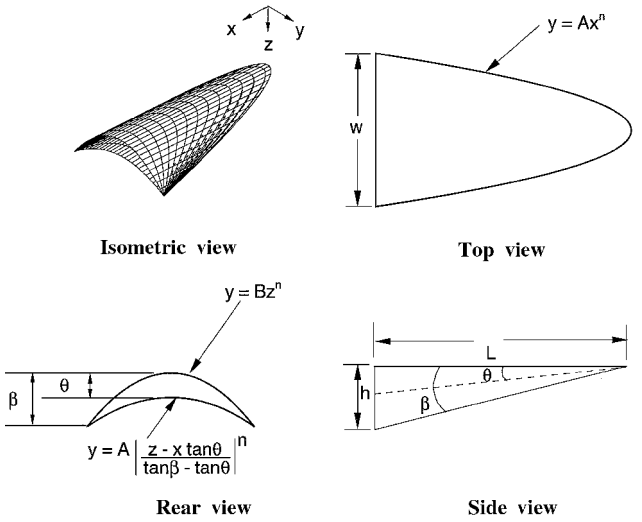

Fig. 1 Parametric vehicle example: w = 9.33 m, l = 50 m, n = 0.5, θ = 5 deg.

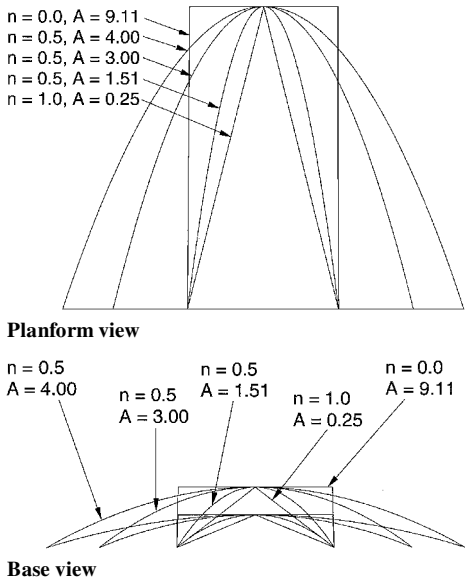

Fig. 2 Geometries created by variations in power-law constant A and exponent n.

application of Eq. (1) between $x = 0$ and the lower surface length, $x = l/\cos\theta$, along with Eq. (3). At a 0-deg angle of attack, the vehicle base plane is taken perpendicular to the flight path and the upper surface is aligned with the freestream. These equations result in five variables (A, B, n, l, and θ) that may be manipulated to generate a wide variety of vehicle configurations.

Small variations in these five parameters can result in large variations in the resulting vehicle geometry, as shown in Fig. 2. A spatulate configuration (blunt planform) with a flattop is generated by setting $n = 0$. It should be noted that at the extreme value of $n = 0$, the waverider becomes unrealistic from a structural standpoint (i.e., infinitely thin shock attachment fins) but is left in the analysis for completeness. The other extreme of $n = 1$ produces the more familiar caret-style waverider.[1]

Waveriders are designed with the assumption of an attached leading-edge shock. Not all variable combinations possible with this parametric geometry will lead to a valid waverider with an attached shock. Shock attachment is guaranteed by setting

$$B = A/\tan^n \beta \tag{4}$$

where the shock angle β must be less than the maximum shock attachment angle. Substituting Eq. (4) into Eq. (3) results in

$$z_l = x\tan\theta + (y/A)^{1/n}(\tan\beta - \tan\theta) \tag{5}$$

for the curvature of the lower surface with an attached shock. When the analysis is restricted to vehicles with attached shocks, the number of variable parameters is reduced to four: A, n, l, and θ.

The vehicle height h and width w are given by

$$h = (A/B)^{1/n} l = l\tan\beta \tag{6}$$

$$w = 2Al^n \tag{7}$$

When Eq. (7) is used, the variable parameters can be changed to a more convenient set consisting of l, w, n, and θ.

All of the generating equations for this parametric model have been derived and validated in previous work[2,3] and are as follows:

$$y_p = Ax^n$$

where $A = w/2l^n$,

$$y_u = B(z_u)^n$$

where $B = A/\tan^n\beta$,

$$z_l = x\tan\theta + (y/A)^{1/n}(\tan\beta - \tan\theta)$$

$$h = l\tan\beta, \qquad w = 2Al^n, \qquad S_p = \frac{wl}{n+1}$$

$$S_b = S_p\tan\theta, \qquad V = \frac{S_b l}{n+2}$$

$$S_{w\infty} = 2\int_0^l\int_0^{x\tan\beta}\sqrt{1+\left(\frac{\mathrm{d}y}{\mathrm{d}z_u}\right)^2}\,\mathrm{d}z\,\mathrm{d}x$$

$$S_{wc} = 2\int_0^l\int_{x\tan\theta}^{x\tan\beta}\sqrt{1+\left(\frac{\mathrm{d}y}{\mathrm{d}z_l}\right)^2}\,\mathrm{d}z\,\mathrm{d}x$$

$$L = S_b[P_b - P_l]\sin\alpha + S_p[P_l - P_u]\cos\alpha$$

$$D_w = S_b[P_l - P_b]\cos\alpha + S_p[P_l - P_u]\sin\alpha$$

$$D_{v,\mathrm{surf}} = G_1 w F(n)\left(\frac{l}{\cos\theta_{\mathrm{surf}}}\right)^{G_2}$$

$$F(n) = F_0 + F_1 n + F_2 n^2 + F_3 n^3$$

The vehicle model is generated with the assumption of two-dimensional streamlines over the body (i.e., no crossflow). The parametric model derived in Ref. 2 analytically defines the viscous drag for either fully laminar or fully turbulent cases by use of the reference temperature method.[4] Eckert's empirical relation is used for the reference temperature along with Sutherland's viscosity law. The constants used for the viscous drag equation D_v are summarized in Table 1. Viscous drags for the upper and the lower surfaces are calculated separately and then summed. The equation for D_v is written in a generic form in which θ_{surf} is the inclination angle for the surface being calculated (i.e., $\theta_{\mathrm{surf}} = 0$ deg for the upper surface and $\theta_{\mathrm{surf}} = \theta$ for the lower surface).

This analytical model was validated with a viscous optimized conical waverider generated by the Maryland Axisymmetric Waverider Program[5] (MAXWARP). A second validation was done at off-design Mach numbers and angles of attack, with Euler validation

Table 1 Viscous drag constants for wedge-derived waverider

Constant	Laminar flow	Turbulent flow
G_1	$0.664\sqrt{\rho_e^2 U_e^3 \mu_e C^*/\rho^*}$	$0.037(U_e)^{1.8}(\rho^*)^{0.8}(\mu^*)^{0.2}$
G_2	0.5	0.8
F_0	0.99845	0.99758
F_1	−0.57529	−0.80941
F_2	0.36737	0.54989
F_3	−0.11939	−0.18247

of an optimized osculating-cone-generated waverider by Takashima and Lewis.[6] Details of these validations are given in Ref. 2.

The implicit drawbacks to this analytical model are as follows: 1) The model is assumed to be a true aerodynamic shape with no losses that are due to engine–airframe integration (a reasonable approximation for this rocket application); 2) there is no pressure leakage that is due to shock detachment; 3) centrifugal lift has been neglected; 4) transverse flow is assumed to be zero; 5) the wall temperature is assumed to be constant; and 6) viscous drag errors increase for more cylindrical vehicles.

The assumption that there is no pressure leakage that is due to shock detachment is one of the fundamental design criteria in the theory of waveriders. Although, at one scale or another, all leading edges display some form of bluntness, the sharp leading-edge assumption has been shown to produce an attached shock on waveriders in experimental studies.[7] For cases in which some leading-edge blunting is required for reducing heating in sustained flight, it has been shown experientially[8] that minimal flowfield degradation occurs (<5% change in L/D ratio).

Inspecting the *L/D* Equation

The equations for lift, wave drag, and viscous drag from Table 1 are used to determine the L/D ratio of the vehicle and then simplified. The final results of the simplification are

$$L/D = L/(D_w + D_{v,u} + D_{v,l}) = 1/(\Psi_1 + \Psi_2\Psi_3\Psi_4) \quad (8)$$

with the dependencies of the Ψ functions given by

$$\Psi_1 = \Psi_1(\theta, \alpha, M_\infty, Z) \quad (9)$$

$$\Psi_2 = \Psi_2(\theta, \alpha, M_\infty, Z) \quad (10)$$

$$\Psi_3 = \Psi_3(l) \quad (11)$$

$$\Psi_4 = \Psi_4(n) \quad (12)$$

where M_∞ is the freestream Mach number and Z is the design or cruise altitude.

For the purposes of this section, the design conditions used are held constant at a flight Mach number of 8 and an altitude of 20 km. The effects of changing M_∞ and Z are investigated at the end of the paper. For fixed M_∞ and Z, the L/D equation becomes a function of only four geometric parameters: θ, α, l, and n. The functions comprising the L/D equation from Ref. 2 are

$$\Psi_1 \equiv (X + Y)/(1 - XY) \quad (13)$$

$$\Psi_2 \equiv \frac{\left(G_{1,u} + G_{1,l}/(\cos\theta)^{G_2}\right)}{(P_l - P_u)(1 - XY)\cos\alpha} \quad (14)$$

$$\Psi_3 \equiv l^{G_2 - 1} \quad (15)$$

$$\Psi_4 \equiv (n + 1)F(n) \quad (16)$$

$$X \equiv \tan\theta[(P_l - P_b)/(P_l - P_u)] \quad (17)$$

$$Y \equiv \tan\alpha \quad (18)$$

The L/D ratio is maximized by minimization of the two components Ψ_1 and $\Psi_2\Psi_3\Psi_4$ in the denominator of Eq. (8). All viscous effects are contained in the Ψ_2 term, whereas all length dependence and power-law-exponent dependence have been decoupled into the $\Psi_3(l)$ and $\Psi_4(n)$ terms, respectively. The function Ψ_1 will be shown to behave more like a wave drag or blockage term and the product of $\Psi_2\Psi_3\Psi_4$ will be shown to behave more like a viscous term. Both of the terms Ψ_1 and $\Psi_2\Psi_3\Psi_4$ also contain some components of lift and wave drag of the vehicle through the variable X, as well as the pressure difference term $(P_l - P_u)$ in Ψ_2.

An important note on the modeling methodology chosen herein is that Eq. (8) is independent of the width of the vehicle. The results presented herein take the form of a similarity solution, in which all vehicles can be tailored to meet specific mission requirements through adjustment of the width. The similarity is an inherent characteristic that is due to the uniform wedge angle of the vehicle and

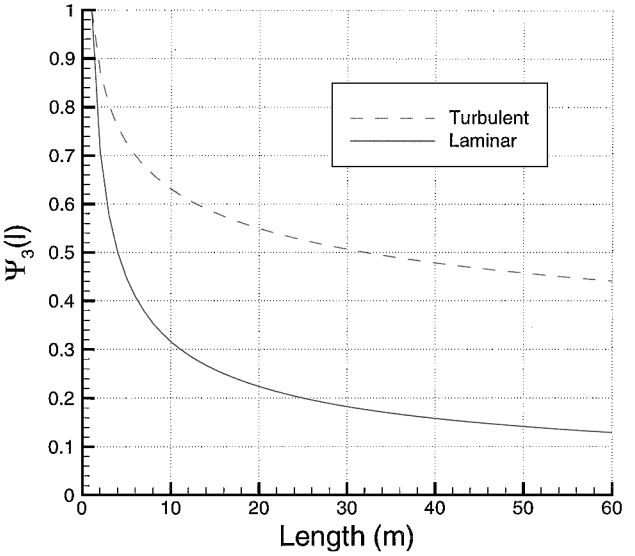

Fig. 3 $\Psi_3(l)$ vs vehicle length l.

therefore to the constant flow properties along each streamline. Also, because the width scales with the constant A for a given exponent n (i.e., $w = 2Al^n$), the width of each stream channel scales by the same constant, thereby scaling the viscous drag linearly in A. Also, the L/D ratio remains independent of width only if shock attachment is maintained; otherwise a three-dimensional flowfield with pressure leakage will develop. When variations in the vehicle's width are used, the vehicle can be tailored to achieve any desired volume, allowing for flexibility in choosing the design geometry. The drawback to deriving assumptions used for this vehicle are that the viscous drag errors increase for more cylindrical vehicles (i.e., long and slender with small radius of curvature). Although this study does not independently investigate the off-design effects on the magnitudes of lift and drag, these will obviously play an important role in the design of an optimum trajectory and influence the design of the propulsion system, structural framework, volumetric packaging, etc. The nature of the similarity formulation prohibits this type of detailed design investigation without significantly increasing the complexity of the study.

Length-Scale Effects

As the length of the vehicle increases, it would be expected that the blockage-dominated term (Ψ_1) would overshadow the viscous-dominated term ($\Psi_2\Psi_3\Psi_4$). This effect is partially confirmed (i.e., the relative decrease in the viscous term) by examination of the plot of the function $\Psi(l)$, as shown in Fig. 3 for both the totally laminar and totally turbulent extremes of viscous drag. From the plot shown in Fig. 3, it is easily seen that as the length increases the bulk effect is to decrease the viscous term, thereby increasing the L/D ratio. Conversely, as the length of the vehicle is shortened (especially below 6 m), the viscous effects begin to grow dramatically and most likely overtake the blockage drag as the dominant term in the denominator.

Planform Shape Effects

Contributing to the effects of viscosity, although not as significantly as the overall vehicle length, is the variation in the average streamline length caused by changes in the power-law exponent n. As the vehicle becomes more spatulate shaped (i.e., planform bluntness increases as $n \to 0$), the average streamline length increases and the contribution of Ψ_4 to the viscous term decreases. This fact is reiterated by Fig. 4 for the function $\Psi_4(n)$ for various values of the power-law exponent n for the laminar and the turbulent viscous drag extremes. It is interesting to note that changing the power-law exponent between $n = 0$ (spatulate) and $n = 1$ (caret) varies the turbulent drag by only ~11%, whereas the spatulate vehicle has twice the planform area and three times the volume of the caret waverider. As the design conditions change or a vehicle is optimized for an

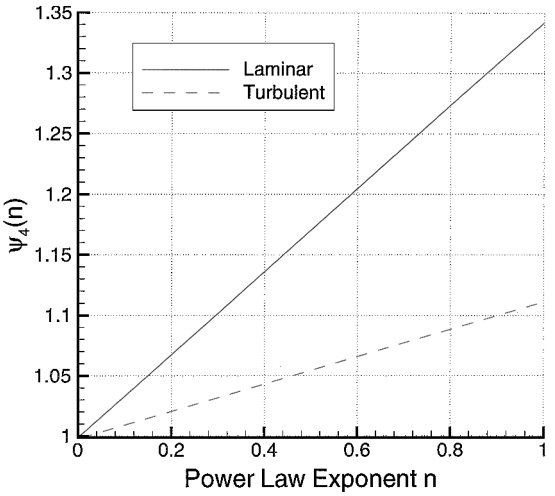

Fig. 4 $\Psi_4(n)$ **vs power-law exponent** n.

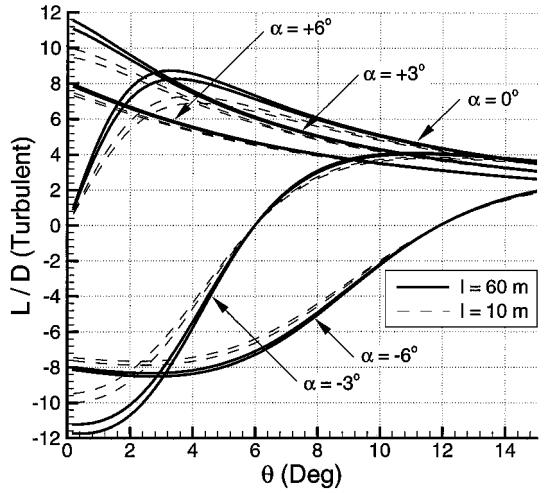

Fig. 5 L/D **ratio vs** θ **with variations in** l **and contours of power-law exponent** $n = 0$ **(top) and** $n = 1$ **(bottom) for** $\alpha = 0$ **deg.**

entire mission trajectory, the transition between laminar and turbulent drag and knowledge of the regions where the drag is entirely laminar or entirely turbulent will become increasingly important. This desire for increased transition information is also emphasized by the fact that the effect of planform bluntness on laminar flow is to decrease the viscous term by 25%.

Although not considered explicitly in this paper, the volumetric efficiency $\eta_{S_w} = V^{2/3}/S_w$ of this model can be maximized by setting $n \approx 0.2$, as shown in Ref. 2. It is in this type of consideration in which the width becomes an important variable in tailoring the design to fulfilling volumetric requirements.

Combined Effects of l and n

Figure 5 shows the overall effects of changes in length and power-law exponent on the L/D ratio for the totally turbulent viscous drag case. The top and the bottom curves for each vehicle length are for $n = 0$ and $n = 1$, respectively. Unless otherwise mentioned, the base pressure on the vehicle is assumed to be equal to freestream pressure for lift and drag calculations. Some important points on Fig. 5 have been summarized in Table 2. The effects of changes in length become noticeable over large ranges [$0.56 \leq \Delta(L/D) \leq 0.59$ for l changing from 30 to 60 m], but increase significantly for small lengths [$1.04 \leq \Delta(L/D) \leq 1.10$ for l changing from 2 to 10 m]. Similarly, the variations in L/D ratios that are due to changes in n are fairly uniform throughout the desired length spectrum. The wedge angle $\theta|_{(L/D)_{\max}}$ (at $\alpha = 0$ deg) for the peak values of L/D ratios does not change significantly for perturbations about a single design length ($\leq$0.25 deg). This angle is governed mainly by the flight Mach number and the altitude, as will be shown later. It is

Table 2 Effects of variations in l **and** n **on** $(L/D)_{\max}$ **and** θ **at** $(L/D)_{\max}$

	$(L/D)_{\max}$		θ at $(L/D)_{\max}$, deg	
l, m	$n = 0$	$n = 1$	$n = 0$	$n = 1$
60	8.72	8.26	3.27	3.45
30	8.13	7.70	3.50	3.68
10	7.28	6.90	3.90	4.11
2	6.18	5.86	4.55	4.80

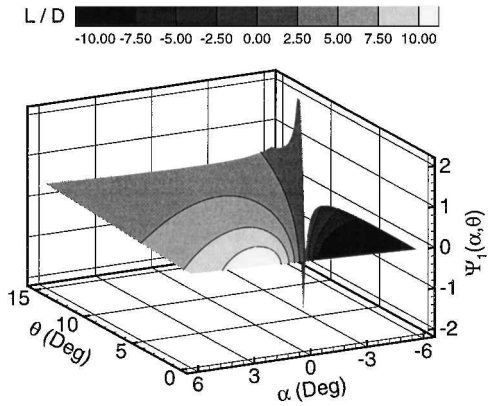

a) Three-axis view with L/D **contours**

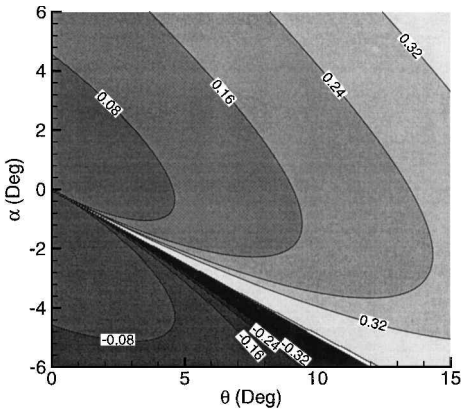

b) α **vs** θ **view with** Ψ_1 **contours**

Fig. 6 $\Psi_1(\alpha, \theta)$ **for variations in** α **and** θ **(**L/D **ratio at** $n = 0$, $l = 60$ **m).**

also of interest to take note of the sharp drop-off in the magnitude of $(L/D)_{\max}$ as the length is decreased.

Figures 5–13 contain data up to a value of $\theta = 15$ deg for consistency and clarity of presentation. It is obvious that, because the maximum value of the L/D ratio is in the vicinity of $\theta \approx 4$ deg, the upper limit of $\theta = 15$ deg will never be approached. The $\theta = 15$ deg upper limit must also be enforced from the position of shock attachment throughout the off-design angles of attack. Because the equations derived herein all assumed total pressure containment associated with shock attachment along the entire leading edge of the vehicle, some restrictions must be made. Lewis and Hastings[9] have shown that at Mach 8 the maximum shock angle β about which perturbations in flight path will move the shock closer to the vehicle as opposed to further away is 15.07 deg. This translates to a maximum wedge angle of 9.54 deg. Above this, with perturbations of the flight path or changes in angle-of-attack, the shock will move away from the vehicle and pressure containment will be diminished. Therefore a maximum wedge angle of 9.54 deg will be imposed as an additional design consideration for the case being studied.

Zero-Degree Angle of Attack

Common waverider vehicle designs align the upper surface of the vehicle with the freestream direction to define the on-design condition (i.e., $\alpha = 0$ deg). This convention is maintained here, although, as will be shown, this is usually not the correct choice.

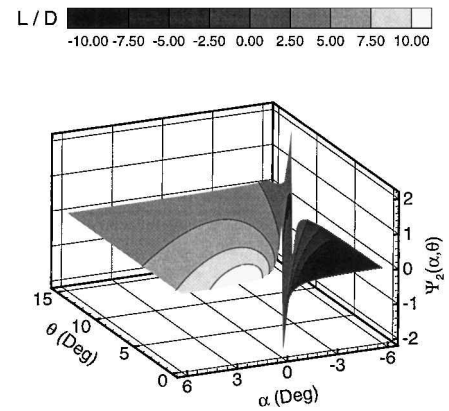

a) Three-axis view with *L/D* contours

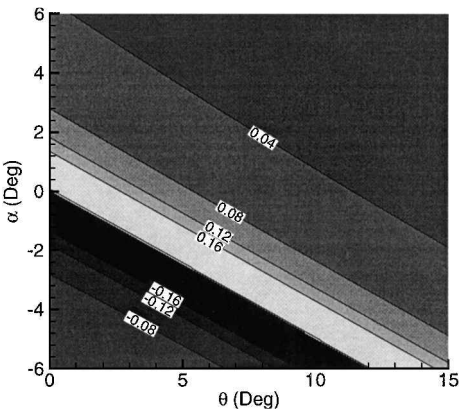

b) α vs θ view with Ψ_2 contours

Fig. 7 $\Psi_2(\alpha, \theta)$ for variations in α and θ (*L/D* ratio at $n = 0, l = 60$ m).

Breaking down Eq. (8) even further for the $\alpha = 0$ deg case results in

$$\left.\frac{L}{D}\right|_{\alpha=0\,\text{deg}} = 1 \Bigg/ \left\{ X + \left[G_{1,u} + \frac{G_{1,l}}{(\cos\theta)^{G_2}} \right] \frac{\Psi_3(n)\Psi_4(l)}{P_l - P_u} \right\} \tag{19}$$

where, as before, the first term in the denominator is the blockage term and the second term is the viscous term, both with a component of lift. Therefore the inviscid limit for the $\alpha = 0$ deg case is

$$(L/D)|_{\text{inviscid}} = X^{-1} \tag{20}$$

which agrees with inviscid oblique shock theory[1] in that, as $\theta \to 0$, $(L/D) \to \infty$. Note that for $P_b = P_u = P_\infty$ this reduces to the more familiar $L/D = (\tan\theta)^{-1}$.

Off-Design Performance

Off-Design Angle-of-Attack Effects

Returning to the L/D equation in the form of Eq. (8), we now discuss nonzero angles of attack. Figure 6 shows the variations of $\Psi_1(\theta, \alpha, M_\infty = 8, Z = 20\,\text{km})$ for changes in θ and α. With the intent of lowering the denominator of the L/D ratio in Eq. (8) in mind, we see in Fig. 6b that the function Ψ_1 increases linearly with θ (for a given positive α) and has a nearly uniform vertical displacement as the angle of attack is increased. This trend agrees with the intuition that as the angle of attack increases positively, the effective wedge angle increases by a similar amount, resulting in a corresponding increase in the blockage term.

Figure 6a also shows L/D contours for the sample case of $n = 0$ and $l = 60$ m. Contrary to the $\alpha = 0$ deg case, the peak L/D magnitude occurs at $\theta < 3$ deg at slightly positive angles of attack. Also, the fact that the achievable range of L/D magnitudes decreases as θ increases is important, again enforcing the fact that a more stable

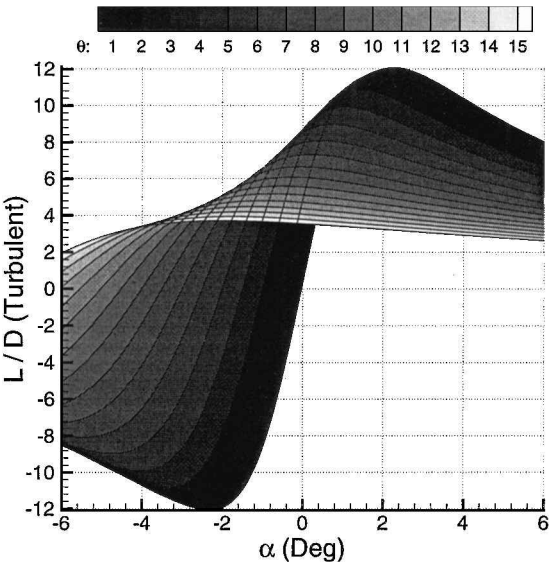

a) *L/D* vs α with θ contours

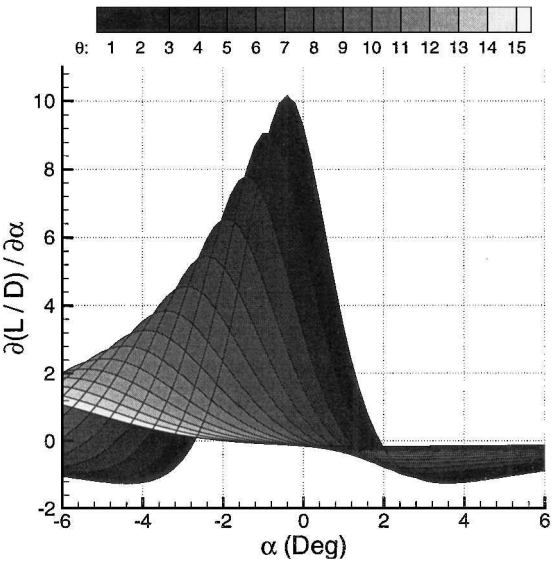

b) $\partial(L/D)/\partial\alpha$ vs α with θ contours

Fig. 8 *L/D* ratios for variations in α with contours of θ (*L/D* ratio at $n = 0, l = 60$ m).

flight environment exists for vehicles with larger wedge angles (as shown in Fig. 5 for $\alpha = 0$ deg).

At $\alpha = -\theta/2$, the pressure term $(P_l - P_u)$ in the denominators of Ψ_2 and X goes to zero, but L/D is still defined. Taking the limit as $\alpha \to -\theta/2$, we find that Eq. (8) reduces to

$$\lim_{\alpha \to -\theta/2} \frac{L}{D} = -1 \Bigg/ \left\{ \frac{1}{Y} + \left[G_{1,u} + \frac{G_{1,l}}{(\cos\theta)^{G_2}} \right] \frac{\Psi_3(n)\Psi_4(l)}{(P_l - P_b) Y \tan\theta \sin\alpha} \right\} \tag{21}$$

The L/D magnitude for Eq. (21) is small because $\alpha = -\theta/2$ is close to the zero-lift angle of attack.

The spikes in the Fig. 6a are due to the instability alluded to in Eq. (21) when $\alpha = -\theta/2$. These spikes actually extend to $\pm\infty$, but were cut off for clarity. In simple terms, as the negative angles of attack are traversed for any given wedge angle, the sudden loss of lift that occurs as $\alpha \to \approx -\theta/2$ (indicated by the spikes in Fig. 6a) causes a rapid fluctuation in the vehicle L/D ratio from cruise down to zero. Unless the vehicle has infinitely precise control and rapid response, this rapid transition makes the vehicle highly sensitive

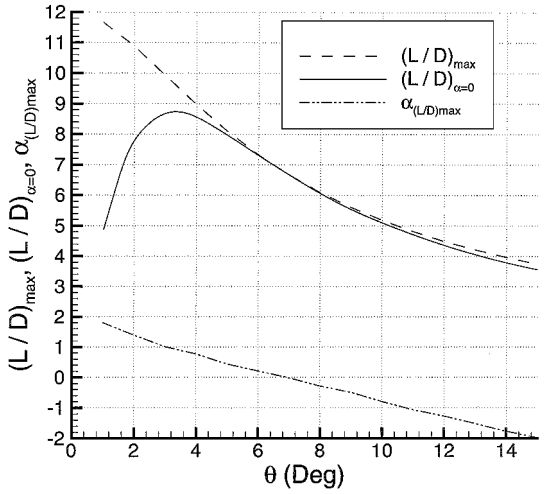

Fig. 9 Angle of attack α that gives peak *L/D* ratio for a given wedge angle θ (*L/D* ratio at $n = 0$, $l = 60$ m).

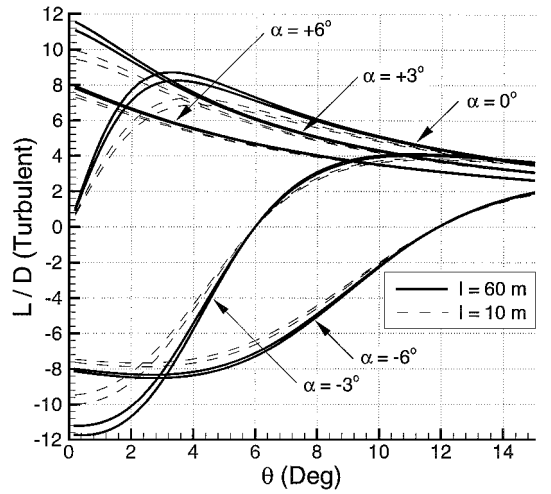

Fig. 10 *L/D* ratio vs θ with bands of angles of attack and contours of *n* and *l*.

around the corresponding angle of attack. Figure 6a also shows that as the vehicle wedge angle increases, the effects of the spike are spread across a larger range of angles of attack, indicating the desire for a larger vehicle wedge angle to minimize L/D sensitivity to α. This result is in opposition to the trends discussed earlier in that the desired vehicle wedge angle for the maximum L/D ratio at $\alpha = 0$ deg is approximately 3–4 deg, whereas the desired wedge angle to minimize angle-of-attack sensitivity is much larger than 4 deg.

In Fig. 6b it is evident that, to minimize Ψ_1 (thereby aiding in maximizing the L/D ratio), small wedge angles are required with angles of attack greater than the zero-lift angle of attack (i.e., $\alpha > \approx -\theta/2$). The fact that at this vehicle length (60 m) the wave drag is the dominant force results in the Ψ_1 contours of Fig. 6a being very similar to L/D contours shown in Fig. 6b.

Figure 7a shows similar trends for Ψ_2 (θ, α, $M_\infty = 8$, $Z = 20$ km) as Fig. 6a for Ψ_1. The effects of angle of attack on Ψ_2 are spread over a larger range around the zero-lift angle of attack for all wedge angles (as opposed to just the larger angles for Ψ_1). These results would tend to reduce the L/D sensitivity to perturbations in α around the corresponding values of α, although Ψ_1 is the more dominant term for 60-m vehicles.

An interesting trend is uncovered in Fig. 7b for Ψ_2 as a function of α and θ; the contours of Ψ_2 move in linear steps perpendicular to the zero-lift spike line. This linearity indicates that in order to minimize the effects of Ψ_2 on L/D the combination of wedge angle and angle of attack must be increased well above the $\alpha = 0$ deg, peak L/D wedge angle.

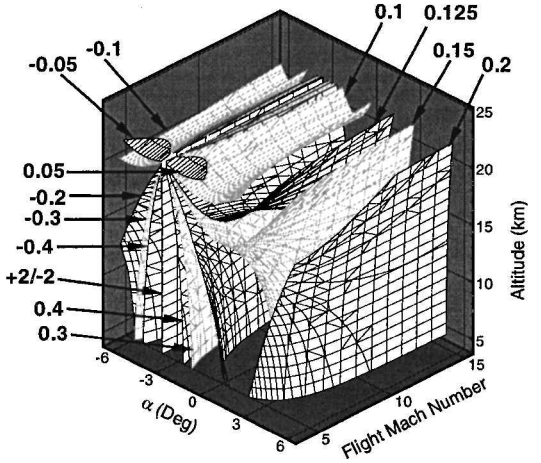

a) Ψ_1 contours

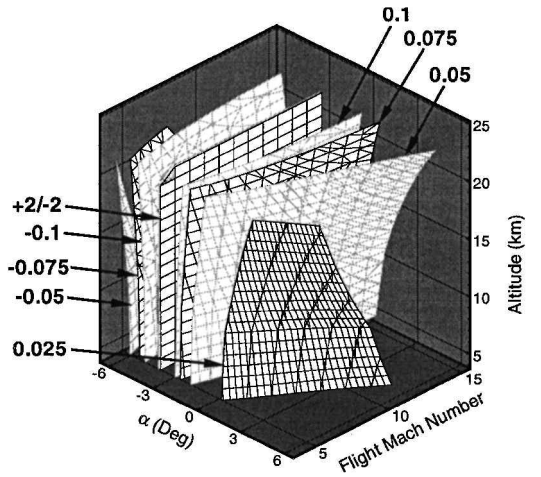

b) Ψ_2 contours

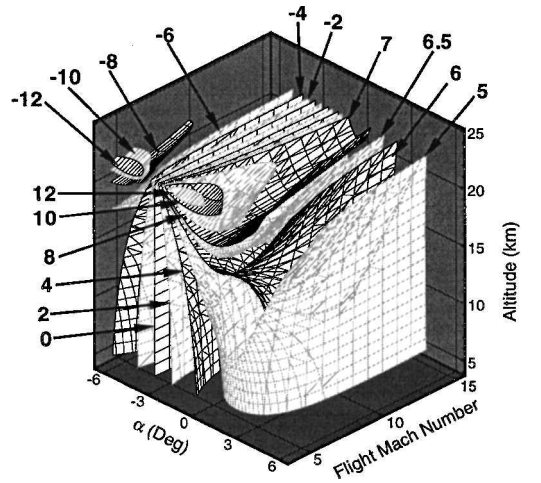

c) *L/D* contours

Fig. 11 Off-design Mach number effects with changes in α and *Z* for a Mach 8 design with $\theta = 6$ deg, $l = 60$ m, and $n = 0$.

The overall effects of the trends in Ψ_1 and Ψ_2 are as follows: 1) to minimize the L/D sensitivity to α in the vicinity of the zero-lift angle of attack, the wedge angle should be larger than the angle for which L/D is maximized, 2) L/D is maximized by small angles θ at small α, and 3) the L/D contours more closely resemble the Ψ_1 contours, indicating that the wave drag term has a domineering effect on the overall vehicle L/D ratio for 60-m vehicles.

We now examine how the L/D ratio is changed for variations in θ and α, as shown in Fig. 8 (for the $n = 0$, $l = 60$ m sample case). It can be seen that the range of possible values of the L/D ratio is

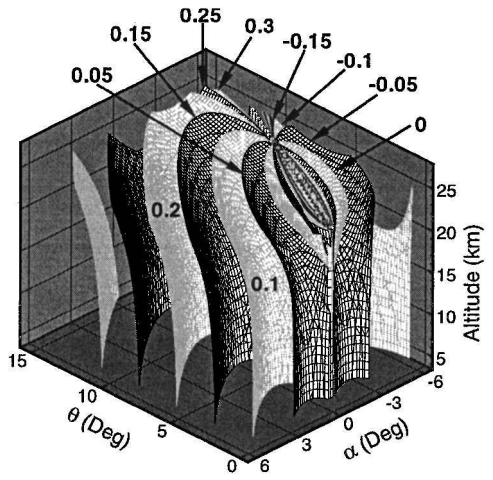

a) Ψ_1 contours

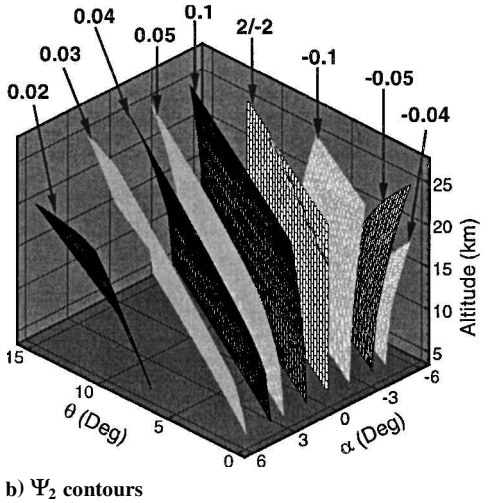

b) Ψ_2 contours

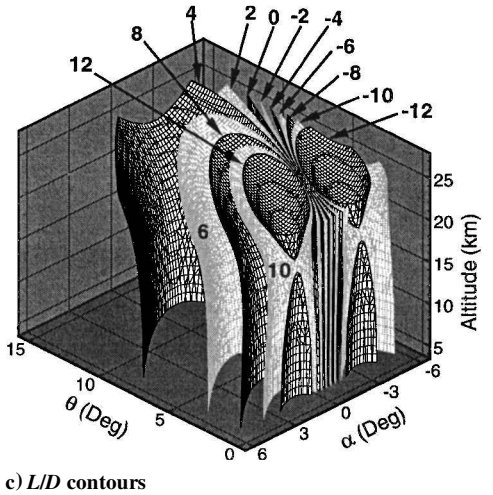

c) *L/D* contours

Fig. 12 Off-design altitude effects with changes in α, θ, and Z for a Mach 8 design with l = 60 m and n = 0.

significantly reduced for the large wedge-angle vehicles. This L/D restriction comes at the expense of a much lower peak magnitude of the L/D ratio.

Figure 8 shows that smaller values of θ produce much larger variations in the L/D ratio of the vehicle through changes in α. From this figure it becomes clear that the largest sensitivities to α are at the smallest angles θ. The peak values of $\partial(L/D)/\partial\alpha$ are at the zero-lift angle of attack for each value of θ. Also, for $\alpha > 2$ deg, the sensitivities of the L/D ratio to α are fairly uniform regardless of θ. We calculate the values of $\partial(L/D)/\partial\alpha$ by sweeping α from -6 to 6 deg.

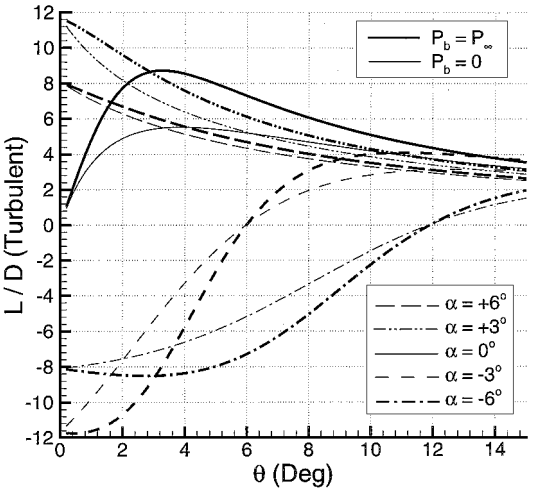

Fig. 13 *L/D* ratio vs θ for varying P_b with l = 60 m and n = 0.

The value of α that gives the peak possible L/D ratio for a given value of θ from Fig. 8a is plotted in Fig. 9. Figure 9 indicates what should be obvious; that the peak L/D ratio for a given value of θ is not always at $\alpha = 0$ deg. Furthermore, Fig. 9 shows that at $\theta = 7$ deg the angle of attack that maximizes L/D transitions from positive to negative. Previous experience in forebody optimization for cruiser-class vehicles[3,5,10] has shown that to maximize both the L/D ratio and the volumetric efficiency the resulting vehicle wedge angle is 5 deg $< \theta <$ 8 deg with a power-law exponent of $n \approx 0.2$, (Ref. 3), indicating that acceptable results could be obtained for vehicle optimization with $\alpha = 0$ deg within this range. In fact, from Fig. 9 it is shown that, for angles above $\theta \approx 5$ deg, optimizing for the maximum L/D ratio at $\alpha = 0$ deg would give minimal error. It should also be noted that at the small Mach numbers, angles of attack, and relatively low altitudes used in this study, the effects of shock-wave/boundary-layer interactions would have a negligible effect on pressure containment.

The culmination of the angle-of-attack effects are summarized by Fig. 10 to include all possible design variations of l, n, and θ. Figure 10 reiterates the findings of Fig. 5 for nonzero angles of attack in that the L/D ratio is relatively insensitive to small changes in the length of the vehicle. Figure 10 also shows that the effect of angle of attack on the L/D ratio over a large variation in vehicle length is maximum for small θ and, more specifically, for $\alpha = 0$ deg at the peak L/D angle. The effects of the power-law exponent n, where n goes from the caret configuration ($n = 1$, curve closest to $L/D = 0$ line for each length and angle of attack) to the spatulate configuration ($n = 0$, curve furthest from $L/D = 0$ line) are also shown in Fig. 10.

Off-Design Mach Number Effects

Recalling that the design point for this vehicle was Mach 8 at 20 km, in this section we look at off-design Mach number and angle-of-attack effects on the vehicle L/D ratio. The Mach number and the angle of attack appear in two of the decoupled components of the L/D ratio in Eq. (8) through Ψ_1 and Ψ_2 in Eqs. (13) and (14), respectively. The off-design effects are shown in Fig. 11 with contours of Ψ_1, Ψ_2, and L/D for parts a, b, and c, respectively. The L/D calculations were generated with the reference case of $l = 60$ m and $n = 0$, along with a constant wedge angle of $\theta = 6$ deg.

Figure 11a shows that in order to minimize the function Ψ_1 (and hence maximize its contribution to the L/D ratio) as the vehicle flies its trajectory it should attempt to reach higher altitudes as soon as possible and fly at speeds lower than the design Mach number (shown by the "cups" in the top part of the figure). This approach would allow the trajectory to be maximized for range through the product of $(L/D)I_{sp}$ in the Breguet range equation. Also, there is clearly an optimum angle-of-attack that will maximize the L/D ratio over the entire altitude spectrum for any given Mach number.

The temperature profile of the portion of the standard atmosphere model[11] used in this study is characterized by two distinct regions:

The troposphere (region closest to the Earth up to 11 km) has a linearly decreasing temperature, followed by the stratosphere that has both an isothermal layer (between 11 and 20 km) and an inversion layer (above 20 km). It is interesting to note that in Fig. 11 the effects of the atmospheric temperature profile are clearly visible at both of the inflection points at 11 and 20 km, respectively.

The temperature effects of the atmosphere are more clearly visible in Fig. 11b for the off-design effects on Ψ_2, as this term is largely temperature dependent (because of the viscous terms). To minimize the variable Ψ_2 it is clear that the vehicle should try to remain as far as possible from the zero-lift angle of attack. Also, as the Mach number is increased for a given altitude and angle of attack, the magnitude of Ψ_2 increases, thereby decreasing the L/D ratio.

Including the off-design effects of both Ψ_1 and Ψ_2 on the L/D ratio, as shown in Fig. 11c, it is shown that the vehicle L/D ratio can be maximized if the altitude is increased as much as possible (constrained by the actual lift requirements) while the cruise Mach number is lowered. The effects of transitioning from the isothermal layer to the inversion layer results in bubbles, in which L/D quickly increases with altitude. Because the variable Ψ_1 is essentially a pressure-dependent variable, the fact that the pressure and the density are decreasing with altitude also contributes to creating the L/D bubbles (i.e., L/D contours closely resemble Ψ_1 contours). It is also interesting to note that a combination of α and Z can be found to maintain a constant L/D ratio through a wide range of Mach numbers. Higher values of L/D ratios can be achieved by overspeeding the vehicle through lower altitudes and then underspeeding at higher altitudes. This approach, of course, is contrary to thermal design requirements, indicating that tradeoffs must be considered.

Off-Design Altitude Effects

The effects of varying Z, θ, and α are shown in Fig. 12 for contours of Ψ_1, Ψ_2, and L/D, respectively, with the design Mach number of 8. Off-design altitude effects on the L/D ratio are generated with the sample vehicle configuration of $n=0$ and $l=60$ m.

In the contours of Ψ_1 in Fig. 12a, the temperature and pressure effects of the atmosphere are visible, although the contour shapes are extremely different from those of Fig. 11a. The interesting result shown in Fig. 12a is that Ψ_1 can be minimized at much larger wedge angles (and for an increasing range of angles of attack) as the altitude is increased. This result is indicated by the cups or bulges centered around the zero-lift angle of attack with the bases extending down to much lower angles θ for low altitudes.

The linear trends shown for Ψ_2 in Figs. 7 and 11b are also visible in Fig. 12b. Once again, the temperature dependence throughout the atmosphere is visible, with clear discontinuities in the magnitude of Ψ_2 at the boundary of the stratosphere. Also, the minimization of Ψ_2 is achieved if a vehicle is designed with a large angle θ to fly with a large angle of attack α at low altitudes or, conversely, with small angle θ to fly with a large negative α at low altitudes.

Combining the effects of Ψ_1 and Ψ_2 with the design case of $l=60$ m and $n=0$ allows the full spectrum of effects on the off-design altitude performance to be determined, as shown in Fig. 12c. As for the off-design Mach contours shown in Fig. 11, the L/D contours in Fig. 12 show a strong dependence on Ψ_1. As indicated for Fig. 12a, the cups in the L/D contours allow for a high value of the L/D ratio to be maintained through a range of angles of attack and altitudes for a given design θ. The range of angles θ that result in high values of the L/D ratio increase as the altitude increases.

Base Drag Effects

Depending on the type of mission and trajectory and the engine type and conditions, the common assumption that base pressure P_b is equal to the freestream pressure P_∞ may be invalid. This study avoided the complex issues of engine performance and engine–airframe integration for waveriders with airbreathing engines by assuming base-mounted rocket engines. Looking through a range of base pressures from freestream (engine on) to nearly vacuum (engine off) for a full range of angles of attack results in the contours as shown in Fig. 13 for the $n=0$ case at Mach 8 and 20 km. It is clearly shown that for base-pressure differences between P_∞ and vacuum the L/D ratio drops significantly for configurations with smaller wedge angles (<9 deg), indicating that correct base-pressure knowledge is essential for a truly trajectory optimized waverider configuration. For vehicles with wedge angles greater than 9 deg, the effects of base pressure for values of -3 deg $< \alpha < +6$ deg are localized to a L/D magnitude change of ~ 1.

Conclusions

Many aspects of waverider design and optimization have been explored through the use of a simple parametric vehicle model. Off-design angles of attack have been shown to have a dramatic impact on the L/D ratio, especially near the vehicle half-angle, indicating that controllability of the waverider from a pure pitching standpoint affects the desired vehicle wedge angle considerably (pushing it higher than the maximum L/D angle). Through decoupling of the L/D equation, it has also been shown that length and planform bluntness effects are evident in only the viscous drag term and that to maximize a vehicle L/D ratio the length should be increased as much as possible and the planform should be as blunt as possible. From a base-pressure standpoint, the vehicle should be designed including off-design base-pressure effects (i.e., engine off) to obtain a truly optimal configuration.

Off-design angle-of-attack and Mach number effects have shown that it is possible to find a combination of angle of attack, altitude, and flight Mach number to maximize the L/D ratio over a trajectory, which should translate to increased range. It was also shown that a vehicle with a design point of Mach 8 and 20 km would show increased performance operating at higher altitudes and lower Mach numbers, provided that the magnitude of lift was sufficient to support steady flight.

Acknowledgments

This research was supported by the Center for Hypersonic Education and Research at the University of Maryland under Technical Monitor Isaiah Blankson of NASA (NASA Grant NAGw 11796), as well as by the Boeing Space Transportation Concepts and Analysis Business Development Division under Technical Monitor Dana Andrews (Boeing Contract JQ4085), the support of whom is greatly appreciated.

References

[1]Rasmussen, M., *Hypersonic Flow*, 1st ed., Wiley-Interscience, New York, 1994, pp. 100–108.

[2]Starkey, R. P., and Lewis, M. J., "Simple Analytical Model for Parametric Studies of Hypersonic Waveriders," *Journal of Spacecraft and Rockets*, Vol. 36, No. 4, 1999, pp. 516–523.

[3]Starkey, R. P., "A Parametric Study of *L/D* and Volumetric Efficiency Trade-Offs for Waverider Based Vehicles," M.S. Thesis, Univ. of Maryland, College Park, MD, June 1998.

[4]White, F. M., *Viscous Fluid Flow*, 1st ed., McGraw–Hill, New York, 1974, pp. 28, 589–592.

[5]Corda, S., and Anderson, J. D., "Viscous Optimized Hypersonic Waveriders Designed From Axisymmetric Flowfields," AIAA Paper 88-0369, Jan. 1988.

[6]Takashima, N., and Lewis, M. J., "Optimization of Waverider-Based Hypersonic Cruise Vehicles with Off-Design Considerations," *Journal of Aircraft*, Vol. 36, No. 1, 1999, pp. 235–245.

[7]Sabean, J., Lewis, M. J., Mee, D., and Paull, A., "Performance Study of a Power Law Starbody," *Journal of Spacecraft and Rockets*, Vol. 36, No. 5, 1999, pp. 646–652.

[8]Gillum, M. J., and Lewis, M. J., "Experimental Results on a Mach 14 Waverider with Blunt Leading Edges," *Journal of Aircraft*, Vol. 34, No. 3, 1997, pp. 296–303.

[9]Lewis, M. J., and Hastings, D. E., "Bow Shock Matching With Viscous Effects on Hypersonic Forebodies," AIAA Paper 89-2678, July 1989.

[10]Takashima, N., "Optimization of Waverider Based Hypersonic Vehicle Designs," Ph.D. Dissertation, Univ. of Maryland, College Park, MD, May 1997.

[11]"U.S. Standard Atmosphere, 1976," National Oceanic and Atmospheric Administration, NASA, U.S. Air Force, Washington, DC, 1976.

M. S. Miller
Associate Editor